Thermal Performance of An Innovative Rotating Fan-Sink Radiator.

Shueei-Muh Lin*, Didi Widya Utama***, Chihng-Tsung Liauh* and Agustinus Purna Irawan**.

ABSTRACT

The cooling device is traditionally composed of two components: (1) the conductive sink and (2) the axial fan. This research proposes a novel design of a rotating fan-sink radiator, with the rotating fan made of conductive material serving two functions: heat conduction and drawing in cold air. The numerical and experimental results for the rotating fan-sink are very consistent; two indexes of its performance are presented: (1) the thermal resistance as low as possible and (2) the ratio of thermal admittance to the required power consumption driving the rotating fan as high as possible. Cooling performance is improved by increasing the relative velocity of the conductive fan and the cooling fluid. The effects of the number of blades, the hub diameter, and the power consumption on heat transfer performance are investigated. This study discovered that the fan-sink's thermal resistance is considerably less than the literature under some parameters. Moreover, the thermal admittance-power consumption ratio is significantly greater than the other. Finally, some correlation formulas for the Nusselt number were established with less than 6% error compared to the experimental data.

* *Professor, Department of Mechanical Engineering, Kun Shan University and Green Technology Research Center (GETRC), Tainan City 710303, Taiwan ROC.*
email: smlin45@gmail.com, liauhct@mail.ksu.edu.tw

** *Professor, Department of Mechanical Engineering, Universitas Tarumanagara, Jakarta 11440, Indonesia.*
email: agustinus@untar.ac.id

*** *Graduate Student, Department of Mechanical Engineering, Kun Shan University, Tainan City 710303, Taiwan ROC.*
email: didiu@ft.untar.ac.id

INTRODUCTION

Heat exchangers are an efficient way for thermal management and temperature regulation. The fins of the heat sink conduct heat from the heat source to the outer surface of the fins. Traditional heatsinks consist of a fixed fin and a rotating fan and require a certain amount of space.

Many researchers are devoted to enhancing the thermal performance of the heat sink, such as studies on generating various geometrical topologies and arrangement of the fins, increasing the surface area of the fins, differentiating the fin's material, and enhancing the cooling fluid flowing throughout the fins (Dhaiban and Hussein 2020, Yunus and Ghajar 2014, Abed and Suker 2021, Kim and Kim 2012, Abdel 2009). In addition to the optimum design of sink geometry, Yang et al. (2013) investigated the performance of a rotating pin-type heatsink with jet impingement of air cooling. However, some fans or blowers need to pump the air jet impingement. Kim and Kim (2012) investigated the performance of a centrifugal heat sink composed of fixed fins with concentric circles and a centrifugal fan. The fan blades are placed between the fins of the circular heat sink. The design of the device was compact but complicated to manufacture.

Staats and Brisson (2015) investigated the device's performance composed of multi-centrifugal fans, heat pipes, and multi-layer heated stators. Obviously, the higher the number of heated stators and centrifugal fans, the lower the thermal resistance. However, the device was very complicated. Koplow (2010) investigated a heat-sink-impeller as a thermal solution that consists of a heat spreader with fins and the hybrid of a conventional finned metal heatsink and an impeller in an arrangement of centrifugal likes fans. The device needs to rotate at several thousand rpm for significant thermal resistance performance.

On a scroll heatsink developed by Kim, T et al. (2008), coolant fluid was pulled into the area between the moving fins and the cooling fixed fins in the scroll heat sink by a relative motion between them, removing heat away from the cooling fins. Furthermore, due to the eccentric shaft and kinematic linkages, the power dissipation for the movement was substantial; thus, the

device's dynamic balance and vibration were significant, especially at high speed.

From previous literature, none of them studied an axial fan type as an integration of the conductive fin as a cooling system. An axial fan can create a significant flow rate compared to the centrifugal/radial fan at the same rotating speed, contributing to the cooling performance. In addition, many cooling devices also use axial fans due to their simplicity Huang and Gau (2012).

A rotating fan-sink is proposed to accommodate the application of a heatsink. The axial fan of the novel device has two main functions: heat dissipation as a sink and pumping the cooled air like a fan. A computational method is used to assess the fan's performance and compare it to experimental data. When a high-confidence computational setup has been built, the fan-sink optimization design procedure is carried out. Theoretical fan power and thermal resistance are utilized as design criteria to determine the best fan design, and both characteristics are used to establish thermal admittance value.

DESIGN APPLICATION OF ROTATING FAN-SINK

In this present study, A rotating axial fan-sink is proposed. A heat source structure in contact with the fan hub inside the hub's center was added. The hub will transport heat from the source to the blade, and as the fan turns, it will pull cold air from the surrounding environment. To transfer the heat from a stationary position to the rotating device in the center of the fan-sink hub, a Rotating Heat Pipe device (RHP) could be used Chan et al. (2015); Li and Liu, (2020).

The commercial CPU cooling fan heat sink is shown in Fig. 1a. The heat source is transferred to the heat sink through heat pipes. The fan rotates, creates airflow to blow the heat sink, and cools down the sinks Choi and Jeong (2016). Fig. 1b illustrates the rotating fan-sink concept in the application and side by side in comparison with the traditional fan heatsink. The stationary heat source is installed on the enclosure surface and delivers heat to the RHP via liquid convection. The RHP also serves as a fan shaft, picking up heat and transferring it to the opposite end as it spins along the fan-sink. The heat is transported to the fan-sink hub at the end of the RHP and dispersed across the blades. At the same time, while the fan-sink revolves, powered by the RHP's electric motor, it draws cold air and cools the blades.
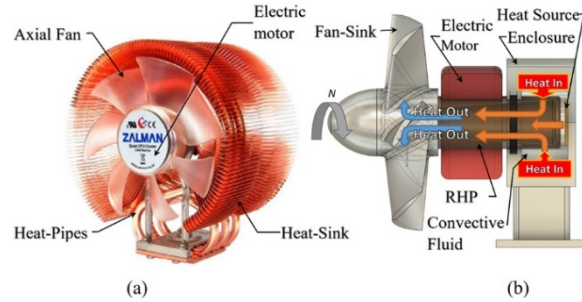
Fig. 1 (a) The commercial CPU cooling fan heat sink (*Zalman LED Aluminum/Copper CPU Cooling Fan CNPS9700: Amazon.ca: Electronics*, n.d.) in comparison to (b) the Fan-Sink concept design.

EXPERIMENT APPARATUS AND PROCEDURES

Axial Fan

A fan-sink with the number of blades n=7 of NACA 4412 blade profile made of aluminum 2024 ($k = 121$ W/mK) has a blade outer diameter D_{fan}=142mm, chord length Lc=35mm, which is measured from the root blade profile. The blade was attached to the hub with a diameter D_{hub}=45mm $\equiv$ D_{hub0} and length L_h=67 mm. The blade setting angle is a=65°; the linear twist angle is b=25°. The blade chord length was reduced by 75% from the root to the tip, as seen in Fig. 2a. A heat source is a cylinder-shaped electric heater with a diameter of d_{ht}=6mm and a length of l_{ht}=20mm located at the hub's center axis and managed under the blade profile's center location to guarantee uniform heat distribution. One of the blade surfaces has four calibrated NTC thermistor sensor point locations for temperature monitoring, which are labeled point tip (T_A), point leading (T_B), point trailing (T_C), and point bottom (T_D), as seen in Fig. 2b. Those sensor's cables are secured by heat-resistant silicone paste, managed by a groove made underneath its blade then pass through a hole connected to the data acquisition module.
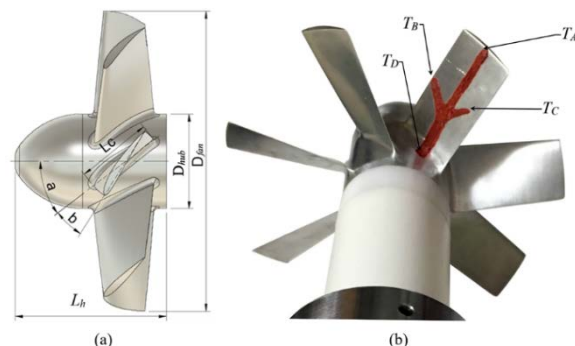
Fig. 2 (a) Fan-Sink design with dimensions, (b) Photo of the actual Fan-Sink with temperature sensors installed.

Fan, Hub & Shaft

As shown in Fig. 3, a fan-sink is attached to a shaft that contains an electronic device for the data acquisition module and its power supply. A 10mm thick Teflon® (k = 0.2 W/mK) insulator spacer was placed between the fan and the shaft to reduce heat transmission from the heat source to the shaft. The shaft is made of POM (polyacetal) to minimize heat conduction and act as an electrical insulator for the electronic device module. The shaft was supported by two needle bearings at the opposite end of the fan blade side to provide stability and preserve a compact bearing housing size. At the end of the shaft, attached carbon material slip-ring assembly for transmitting Q=40 W of electrical power from the power source to a heater. This slip ring system functions as a sliding electrical contact, transferring power from stationary carbon brushes to a spinning electrical conducting ring and then to the heater via wires. An ESP32 microcontroller was utilized as a data acquisition module, sending the measured temperature data from the calibrated thermistor to the laptop at 0.5s interval timesteps through a wireless Bluetooth connection. A transparent insulator (k=0.17 W/m K) was employed as a fan shroud D_c=144mm to address the ease of observation and insulation. The upstream length is 1.5 times the diameter of the fan blade, while the downstream size is 1.0 times the diameter. The shroud has a cone-shaped inlet funnel to improve airflow direction uniformity and a temperature sensor to measure inlet air temperature. During the experiment, an anemometer is mounted to monitor the inlet air velocity passing through the shroud. To illustrate the experiment arrangement, Fig. 4 depict the physical experimental setup.
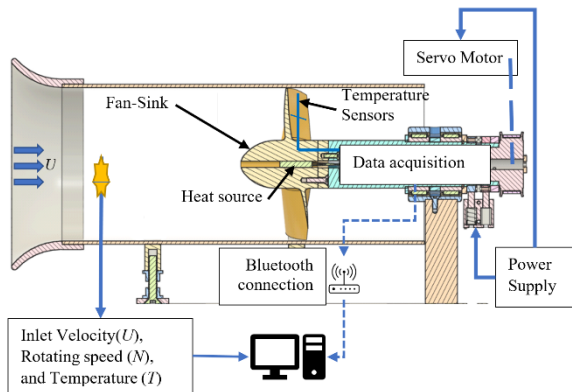
Fig. 3. Experiment physical diagram and setup of the Fan-Sink.

Experiment Procedure

A thorough checklist, including mechanical and electrical components, measuring equipment and sensors, and the data logger, was completed to guarantee that the experiment ran well and accurate data was captured. The fan-sink is rotated to an initial rotating speed of 300 rpm, and the heater is activated. During the fan-sink's rotation, the inlet velocity U,

rotating speed N, inlet temperature T_∞, and heat source Q are monitored. The temperature of the blades (T_A, T_B, T_C, and T_D) was monitored by the data acquisition module. All experiment data was recorded until the temperature variations were insignificant for some period of time. During the experiment, the rotating speed of the fan-sink was used from 300 to 1,000 rpm with a 100 rpm increment.
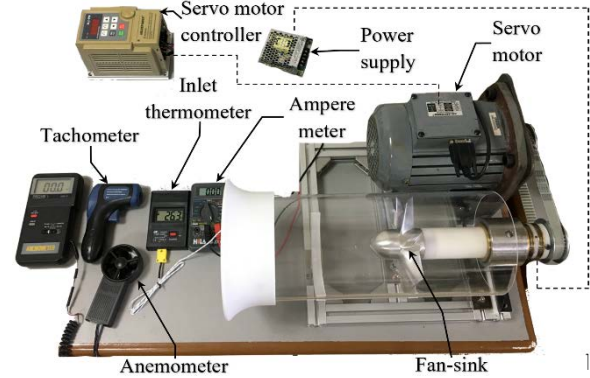
Fig. 4. Actual photograph from the experimental setup of the Fan-Sink.

Errors and Uncertainty Analysis

In this study, some errors and uncertainty are considered from the measured values of the experiment data. Any precautionary measures are also taken while doing and preparing the experiment data; errors are considered from the instrumentations, human reading, and environmental conditions. Table 1 presents uncertainty from the measurement, according to Taylor and Thompson (1998).
The uncertainty of all the measured parameters in the experiment is calculated and listed in Table 1.

Table 1. Experiment's uncertainty

Measured values	Uncertainty value
Measured Distance	±0.07%
Temperature measured	±1.00%
Air velocity measured	±3.00%
Rotating speed measured	±0.02%
Electrical current measured	±0.05%
Heater resistance measured	±0.05%
Electric Power (W) measured	±0.08%
Average Temperature measures	±0.50%
Thermal *convective* coefficient	±0.02%
Nusselt number	±0.07%
Thermal resistance	±0.44%

COMPUTATIONAL AND MATHEMATICAL FORMULATION.

The numerical simulation framework prepared in this study utilized the software Star-CD Lin et al. (2015), and multiple computational domains were employed. In CFD analysis, a set of assumptions was employed to define the computational domains, which are:

• Steady-state analysis
• k-ω SST turbulence model
• Incompressible flow
• Constant properties on fluid and solid domain material
• Non-slip wall condition
• All channel surfaces exposed to the surroundings are assumed to be thermal isolated.

Continuity, momentum, and energy equations of Newton fluid and the conduction equation based on Fourier's law in Cartesian coordinates are Kundu et al. (2012),

Continuity equation

$$\frac{\partial \overline{u_i}}{\partial x_i} = 0 \quad, \tag{1}$$

Momentum equation

$$\frac{\partial}{\partial x_j}\left(\rho u_j u_i - \tau_{ij}\right) = -\frac{\partial p}{\partial x_i}, \tag{2}$$

Where u_i is the velocity in the x_i component, p is the static pressure, ρ is the density of the fluid, and τ_{ij} is the stress tensor. The stress and strain tensors can be expressed as

$$\tau_{ij} = 2\mu s_{ij} - \frac{2}{3}\mu\frac{\partial u_k}{\partial x_k}\delta_{ij} - \rho\overline{u_i'u_j'} \,, s_{ij} = \frac{1}{2}\left(\frac{\partial u_i}{\partial x_j} + \frac{\partial u_j}{\partial x_i}\right), \tag{3}$$

Where u' is the disturbance value of average velocity, δ_{ij} is the Kronecker delta, and $\rho\overline{u_i'u_j'}$ is the Reynolds stresses.

Conduction equation for solid

$$\frac{\partial}{\partial x_i}\left(k_s\frac{\partial T}{\partial x_i}\right) = 0 \quad, \tag{4}$$

The energy equation for fluid

$$\rho\overline{u_j}\frac{\partial\overline{T}}{\partial x_j} = \frac{\partial}{\partial x_j}\left[\left(\frac{\mu_i}{\sigma_i} + \frac{\mu_t}{\sigma_t}\right)\frac{\partial\overline{T}}{\partial x_j}\right]. \tag{5}$$

The $k\text{-}\omega$ SST turbulence model Menter (1994) was employed in the CFD analysis because it could provide integrated balance for predicting near-wall and free-stream problems Argyropoulos and Markatos (2015).

The finite volume method is used to set up the computational domains; the domains consist of fluid static, rotating, and solid domains. The polyhedral mesh type depicted in Fig. 5a with 2.9 million cells is used because an independent study of the mesh reveals that the variance in input velocity and the average temperature has less than 1% difference compared to

the finer mesh size depicted in Fig. 5b. In addition, the mesh close to the wall is improved to satisfy to the SST k- turbulence model when y+ 1.0. Consider the boundary conditions seen in Fig 5(a), the inlet is a stagnation pressure, and a zero-gauge pressure is provided to the outlet surface; all wall conditions, including the fan-sink, are non-slip.

(a)

(b)
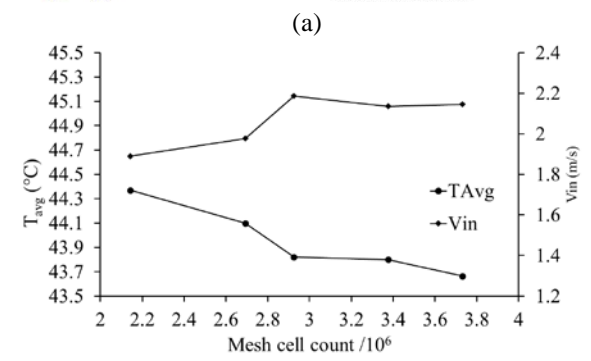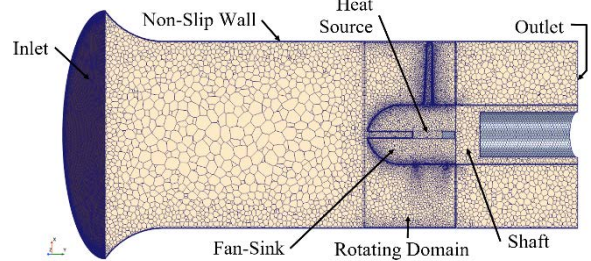
Fig. 5. (a) Cross-section view of the boundary condition and polyhedral mesh of the numerical simulation (b) mesh independent study on T_{avg}, V_{in} for N=1000rpm.

The hub's center receives a total heat source of 40W. A moving reference frame approach is used for the rotating domain, having rotating speed N as an input parameter. The data obtained from the CFD and compared to the experiment include the velocity and temperature inlet, the Fan-sink's rotating speed, and four points probe at the exact position of the physical conditions on the blade. Furthermore, the findings of the comparison between CFD and the experiment are agreed upon and will be published later in this work.

The Reynolds number calculation is based on the following equation:

$$Re = \frac{\rho U D_c}{\mu}, \tag{6}$$

where ρ is the fluid density, U is the inlet air velocity, D_c is the hydraulic diameter (fan's shroud diameter), and μ is the fluid's dynamic viscosity.

The general form of heat transfer correlation is used in the following equation:

$$Nu = CRe^m Pr^n, \tag{7}$$

where Nu, Re, Pr are Nusselt number, Reynolds number, and Prandtl number, respectively, and C, m, n

are the constants obtained from the experimental empirical study.

During the analysis of the experiment data to calculate the heat source, the following equations are used:

$$Q = R_{ht} I^2 ,$$
(8)

where Q is the total heat source of the heater, R_{ht} is the measured resistance of the heater, and I is the measured electrical current flowing.

In the experiment, the temperatures $\{T_A, T_B, T_C, T_D\}$ at four position points of the blade are measured, as shown in Fig. 2b.

The average heat convection is expressed as

$$Q_{avg\,conv} = h_{avg\,exp} A_s \left(T_{avg} - T_\infty \right) ,$$
(9)

where $h_{avg\,exp}$ is the average heat transfer coefficient, A_s is the surface area of the fan-sink, T_{avg} is the average temperature of the fan-sink, and T_∞ is the inlet temperature of the cooling fluid.

The experiment average Nusselt number is expressed as

$$Nu_{avg\,exp} = \frac{h_{avg\,exp} D_c}{k} ,$$
(10)

where k is thermal conductivity, and D_c is the hydraulic diameter as a characteristic length.

In general, the thermal resistance of the Fan-Sink can be defined as:

$$R_{heat} = \frac{T_{max} - T_\infty}{Q} ,$$
(11)

where T_{max} is the temperature at the heat source and the inlet cooling air's temperature.

RESULTS & DISCUSSION

In this study, the thermal performance of the existing fan-sink design is compared with that of the computational method. Temperature, rotating speed, inlet velocity, and the heat source are measured experimentally and compared to CFD. The heat performance of the fan-sink device concerning the Nusselt number and correlation equation is also presented. The fan-sink thermal performance is evaluated in conjunction with the fan power and utilized as a benchmark to build a new fan-sink design to get the optimal configuration with good thermal performance while maintaining low power consumption.

Comparison of The Numerical and Experimental Results

The input velocity is measured to determine the aerodynamic performance of the fan-sink. The average velocity is proportional to the fan's rotating speed, as seen in Fig. 6. Moreover, the inlet velocity obtained by CFD and experimental methods is quite similar.

Fig. 7 depicts the cross-sectional temperature distribution and velocity vector of the fan-sink CFD result (Q=40W, D_{hub} = 45mm, l_{ht} = 20mm, D_{fan} =142mm, n=7, N = 1000 rpm). Observing temperature differences from the middle of the hub to the blades shows that the junction of the heater and the hub has the maximum temperature, while the blade tip has the lowest temperature.

As seen in Fig 7, the insulating spacer is also efficient in limiting heat transfer to the shaft, indicating that heat can be dispersed between the blades and the hub. However, the maximum temperature is near the heat source, and it appears that the hub is not able to efficiently transmit heat to the blades.
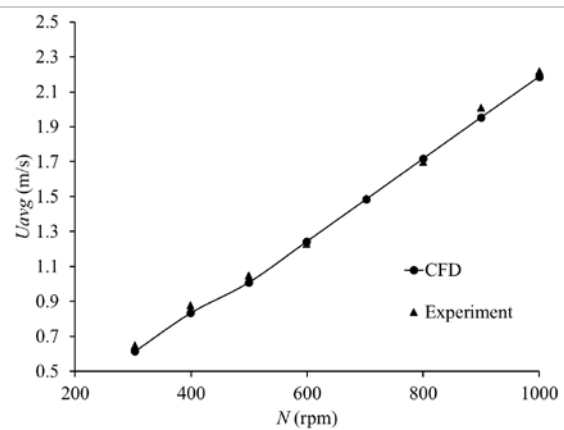
Fig. 6. Comparison between CFD and experiment data for average inlet velocity U_{avg} at various rotating speeds N.
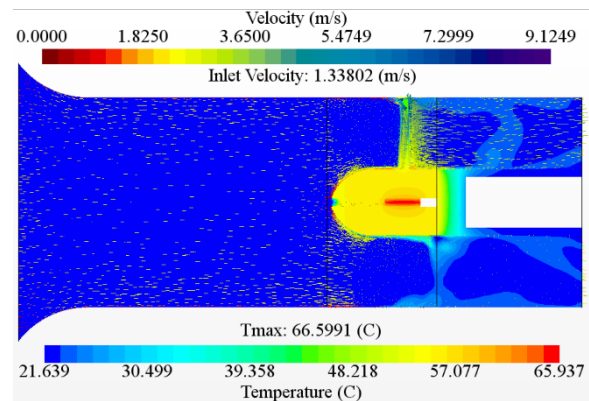
Fig. 7. CFD result of the temperature distribution on the solid domain and velocity vector on the fluid domain.

The velocity vector demonstrates that convective heat transfer has occurred successfully between the blades and continues to the downstream region, resulting in the quick evacuation of hot air.
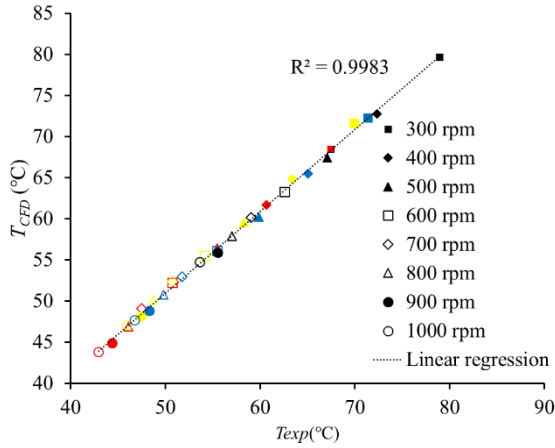
Fig. 8. Temperature data on the blade compared between CFD (T_{CFD}) and experiment (T_{exp}) at varying rotating speeds N.

Aside from velocity, temperature is an essential metric that is measured.

Fig. 8 depicts a comparison between CFD and experimental temperature data (T_A, T_B, T_C, dan T_D). Linear regression is used to examine the consistency of CFD and experimental results. As seen in

Fig. 8, both data are consistent with $R^2=0.9983$ and the maximum percentage of error of less than 4%. Fig. 9 compares the average experiment heat convective coefficient to the computational method, which has a maximum deviation of 4.5 percent. The greater heat convective coefficient correlates to the increased fan rotating speed represented by the increasing Reynold number.

The experiment average Nusselt number is derived from the experimental data using Eq. (7) and compared to the CFD approach. Its correlation has a maximum inaccuracy of 5.6 percent; thus, the general correlation formula for the average Nusselt number to the fan-sink device can be obtained from Eq. (7), as shown below:

$$Nu_{avg\,exp} = 2.1535 Re^{0.489} Pr^{\frac{1}{3}} \qquad (12)$$

where the range of Reynolds number is $5500 < Re < 23000$. The Nusselt number indicates the performance of convective heat transfer; the higher Reynolds number corresponds to the higher Nusselt number for the Fan-Sink. Fig. 10 depicts the changes in Nusselt number as a function of Reynolds number between the experiment data, CFD data, and correlation equation Eq (12). The maximum error is less than 5%, which indicates that the experimental data and CFD data are consistent.
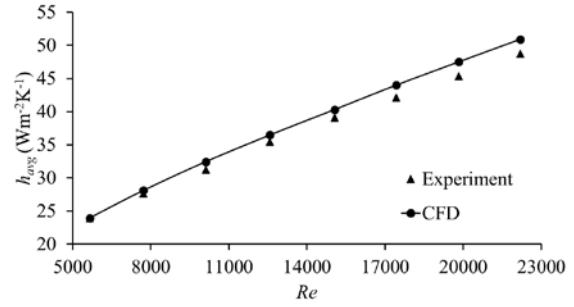
Fig. 9. Correlation between Reynolds number and average heat convective coefficient h_{avgexp} on experimental and CFD data.

The moment (M) values derived from CFD data are used to calculate the fan mechanical power (P_{fan}) required to rotate the fan-sink device at a certain rpm. The equation below is used to calculate the moment:

$$M = \sum_f \left[r_f \times \left(F_f^{pressure} + F_f^{shear} \right) \right] a_x \qquad (13)$$

where $F_f^{pressure}$ and F_f^{shear} are the pressure and

shear force vectors, and a_x is a vector, defining the axis through point X_0 about which the moment is taken and is the position of face f relative to the X_0.
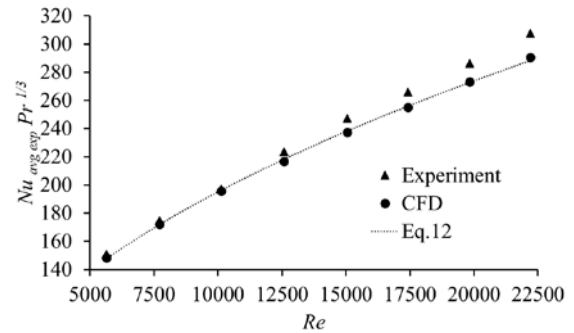
Fig. 10. Correlation of the Reynolds and Nusselt numbers on the experimental data, CFD data, and eq (12).

Furthermore, since the moment is obtained from the above equation, then the fan power (P_{fan}) can be easily found using the following equation:

$$P_{fan} = \frac{M \pi N}{30} \qquad (14)$$

where N is the rotating speed per minute of the fan-sink. One of the design criteria derived from Eq. (11) is thermal resistance, which correlates to the fan power. The design will be considered good if it has the lowest thermal resistance and fan power. Fig. 11 demonstrates the power required to drive the fan-sink with the number of blades $n=7$ on the thermal resistance.

It is commonly known that the higher the fan's rotating speed, the greater the power consumption driving the fan-sink. According to Fig. 11, as the fan begins to rotate, the thermal resistance substantially decreases. When the power consumption exceeds 0.4 W,

the thermal resistance decreases steadily.
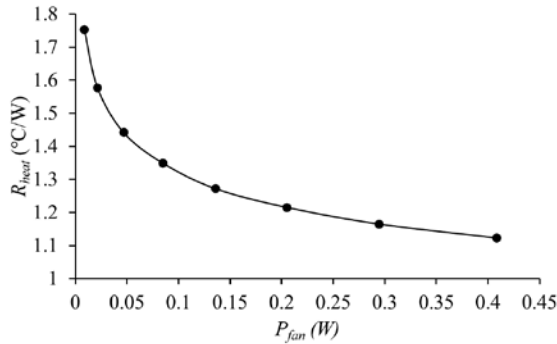
Fig. 11. Fan power consumption P_{fan} correlated to the thermal resistance coefficient R_{Heat}.

It indicates that when the rotating speed exceeds the critical value, the heat transfer efficiency is nearly constant. The thermal resistance is 1.12 °C/W when the power consumption is 0.41W, and the corresponding rotating speed is 1000 rpm.

Table 2. Fan-Sink new design dimension parameters

No.	Hub ratio ($D_{hub} = \alpha D_{hub0}$)	Hub-to tip-ratio	Hub diameter D_{hub} (mm)	Heater diameter d_{ht} (mm)
1	$\alpha = 1.0$	3.20	45.00	39.00
2	$\alpha = 1.25$	2.54	56.25	50.25
3	$\alpha = 1.5$	2.12	67.50	61.50
4	$\alpha = 1.75$	1.82	78.75	72.75
5	$\alpha = 2.0$	1.59	90.00	84.00

NEWLY DEVELOPED FAN-SINK DESIGN (EFFECT OF SEVERAL PARAMETERS ON HEAT TRANSFER).

It is common that thermal performance increases as surface area increases. Furthermore, the uniform distribution of surface area can increase the thermal performance of the heat sink Ong et al. (2017). The fan-sink in this present design has a total surface area of As = 0.0331m^2 and comprises 70.6 percent blade surface and 29.4 percent hub surface. To improve the thermal performance of the fan-sink, the number of blades n is raised from 7 to 20. Furthermore, to evaluate the influence of the hub diameter on heat transmission, additional factors such as the fan's outer diameter D_{fan}, blade profile type, blade setting angle a, blade twist angle b, blade profile chord length L_c, heater length l_{ht}, and hub length L_h are held constant. In Table 2, the base parameter D_{hub0} corresponds to the new hub dimension D_{hub} and as hub ratio is presented. Based on these

parameters, the new Fan-sink design is developed.
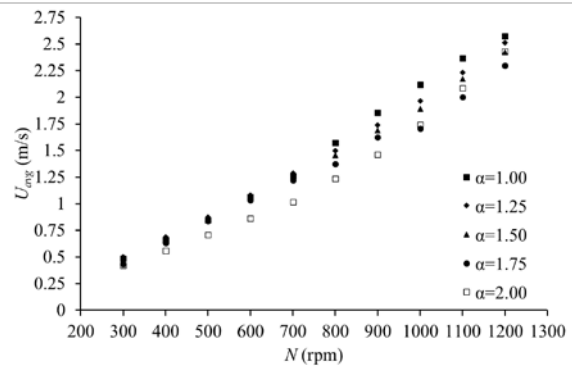
Fig. 12. The effects of the rotating speed N and the average inlet velocity U_{avg} on the hub ratios α.

Figure 7 shows that the distance between the heater surface and the blade was relatively large, meaning that the temperature differences between the heater junction and the hub surface are also significant. This difference indicated that heat was transmitted to the cooling fluid through the blades reasonably slowly. This new design incorporates a decrease and consistent 3 mm hub thickness to address the previous issues. The fluid flow needs to be analyzed as the number of blades increases; Fig. 12 shows that the average inlet velocity is proportional to the fan's rotating speed: the larger the hub diameter D_{hub}, the greater the average intake velocity U_{avg}. The velocity characteristics are equivalent to the previous experimental fan-sink, although the velocity value is considerably lower in this new design; however, the blade surface area has been increased, and the effect correlates to the rise in temperature. The temperature distribution on the surface of the rotating fan-sink with a hub ratio of (α=2, Q=40W, D_{hub}=90mm, l_{ht}=20mm, D_{fan}=142mm, n=20, N=1200rpm) is shown in Fig. 13(錯誤! 找不到參照來源。a), and more blades indicates that the temperature distribution around the blades is generally well dispersed. The highest temperature, however, is found at the hub surface near the shaft. This happens because substantial heat convection occurs when cooling air flows between the fan blades, raising the temperature of the downstream air. As a result, the highest temperature occurs near the end of the hub surface. The velocity vectors depicted in Fig. 13(b) show that the streamline's path causes a swirl effect due to the rotating of the fans, and this provides further improvements in the cooling performance Zhang et al. (2019).

Figure 14 illustrates how the number of blades and hub diameter influence the thermal resistance as a result of the rotating speed (l_{ht} = 20mm, D_{fan} = 142mm). The n=20 thermal resistance value is significantly lower than the n=7 thermal resistance value, and both exhibit the same characteristic of decreasing thermal resistance as the rotating speed rises. Additionally, the effect of hub diameter on heat resistance is insignificant.

Fig. 15 shows the effects of the rotating speed and the hub diameter on the average temperature of the blade. D_{hub} It is found that the higher the rotating speed N, the lower the average temperature of the blade. However, the effect of the hub diameter D_{hub} on the average temperature is negligible.

Tmax: 35.1409 (C)

(a)

(b)
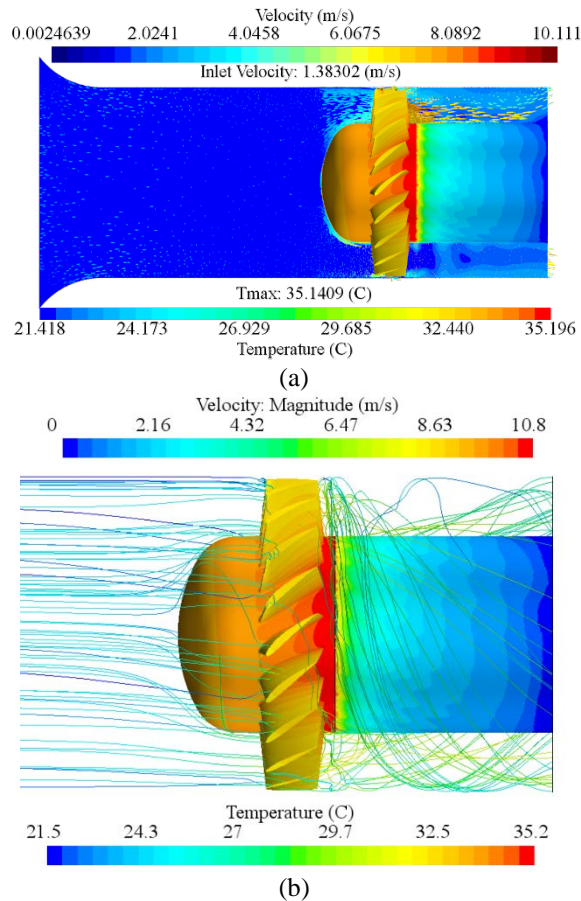
Fig. 13. Distribution of temperature and velocity analyzed by CFD: (a) in the global domain, and (b) streamline of the rotating fan-sink device
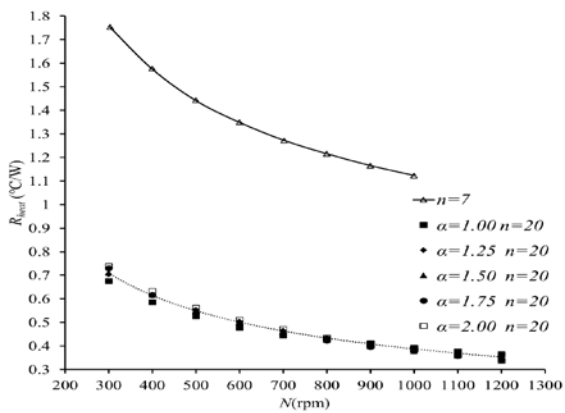
Fig. 14. Effects of the rotating speed N, the number of blades n, and the hub ratio α on the thermal resistance.

The fan-sink ratio is calculated by dividing the

thermal admittance $1/R_{heat}$ by the necessary power consumption P_{fan}. $Y_p = (1/R_{heat})/P_{fan}$ is one index for estimating fan-sink performance. The better the performance, the higher the thermal admittance-power consumption ratio. Fig. 16 depicts the effect of the hub diameter D_{hub} and the power consumption of the fan with $n=20$ blades on thermal resistance ($l_{ht} = 20mm$, $D_{fan} = 142mm$). The lower the thermal resistance, the greater the power consumption, and when the power consumption exceeds 0.9W, the thermal resistance approaches constantly.
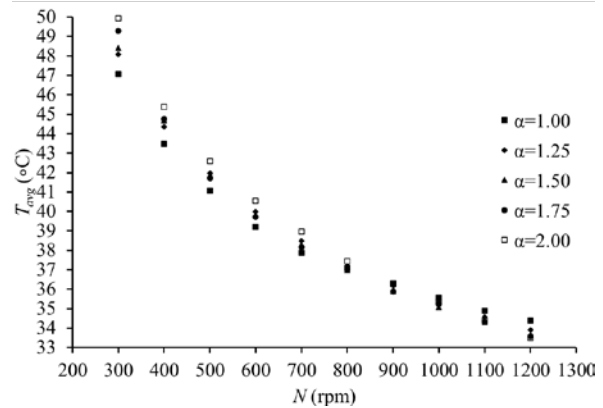
Fig. 15. Effects of the rotating speed N and the hub ratio α on the average temperature T_{avg} of the fan-sink.

The highest thermal performance of the fan-sink at a hub ratio α=2.0 can achieve a minimum thermal resistance of 0.34°C/W at 1200 rpm while consuming 0.97W of electricity. The corresponding thermal admittance-power consumption ratio is Y_p =3.05. At the hub ratio of α =1.25, the power consumption is 0.38W, the thermal resistance is 0.41 °C/W, and the corresponding thermal admittance-power consumption ratio is close to 6.42. Furthermore, Fig. 14 shows that the thermal resistance with n =20 is much lower than with n =7.
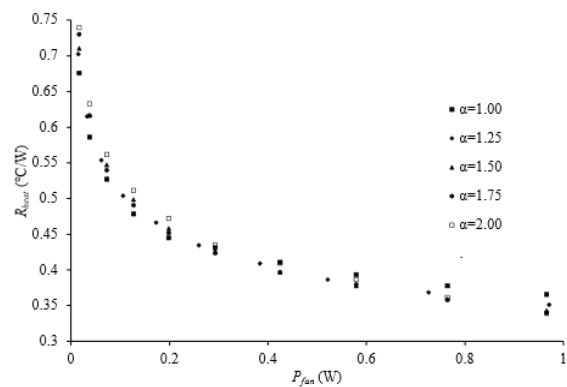
Fig. 16. The effects of the hub ratio α and the fan-sink's power consumption P_{fan} on the thermal resistance R_{heat}

The performances of several similar devices (Kim and Kim 2013, Kim et al. 2008, Staats and Brisson 2015, Koplow 2010), as well as the commercial

heatsink studied by Choi and Jeong. (2016) are compared with the presented study and listed in Table 3. It is found that the thermal resistance of the present study with $n= 20$ is significantly less than that from the literature studies. The minimum power consumption with ($n = 20$, $\alpha =1.25$) is 0.38W, and the maximum thermal admittance-power consumption ratio is close to $Y_p=6.42$. In other words, the performance of thermal admittance is great under the minimum power consumption.
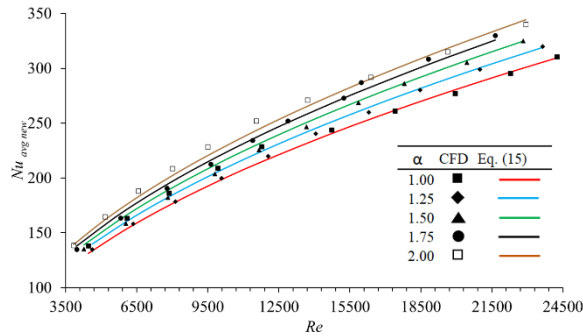
Fig. 17. Relationship between the Nusselt number and the Reynolds number on the hub ratio α.

A comparison of the heat performance to the commercial CPU cooling fan heat sink CPNS-9700 from Zalman Tech was also performed; from Table 3, both performances are close to each other in relatively similar overall dimensions. Nevertheless, this commercial heatsink has more complexity to manufacture and needs more effort in maintenance due to the buildup of dust fouling in between its fins which will be degraded the performance in the long run.

Table 3. Performance comparison of the newly developed Fan-Sink to some previous studies

Fan-Sink Type	Thermal resistance R_{heat} (°C/W)	The required power to rotate the fan P_{fan} (W)	Thermal admittance - power consumption ratio $Y_p=(1/R_{heat})/P_{fan}$	Fan rotating speed N (rpm)
$n = 7$ Blade (experiment)[#] $D_{hub}=D_{hub0}=45mm$	1.12	0.41	2.18	1000
$n = 20$ Blade[#] α=1.25	0.41	0.38	6.42	900
$n = 20$ Blade[#] α=2.0	0.34	0.97	3.05	1200
Centrifugal heatsink Kim and Kim (2013)	0.47	1.82	1.17	1100
Scrolled heatsink Kim et al. (2008)	0.57	-	-	500
Interdigitated single impeller heat sink Staats and Brisson (2015)	0.84*	0.40*	2.98	3000
Single unshrouded centrifugal fan-sink Koplow (2010)	0.22	1.8	2.52	5000
Commercials heatsink CPNS-9700 from Zalman Tech Choi and Jeong (2016)	0.36	-	-	1700

#: In the present study.
*: Result was obtained from heat transfer and power correlation equation given by the author.

Fig. 17 demonstrates the correlation between the Nusselt number and the Reynolds number ($l_{ht} = 20mm$, $D_{fan} = 142mm$, $n = 20$). It is found that the larger the Nusselt number, the greater the Reynolds number. Moreover, the larger the hub diameter, the larger the Nusselt number. The correlation among the Nusselt number Nu_{avgnew}, the Reynolds number Re, the Prandtl number Pr, and the ratio of the fan and hub diameters D_{fan} / D_{hub} is derived as:

$$Nu_{avg\,new} = 2.5918 Re^{0.5059} Pr^{0.3202} \left(\frac{D_{fan}}{D_{hub}} \right)^{-0.1942} \quad (15)$$

where the range of Reynolds number is $3500 <Re<25000$. This formula correlation is also compared to the CFD simulation result and has a maximum of less than 6% error.

The maximum value of the Nusselt number found in Fig. 17 has a much higher value compared to the literature. Additionally, previous studies found that cooling fluid has a significant role in increasing the thermal performance of a cooling device Lin et al., (2015). Therefore, we are eager to continue the current investigation for future research employing a variation on cooling fluid and analyzing its performance.

Since the optimal fan-sink design has been established, it may also be applicable to the various forms of heat exchangers as an alternate option. Potentially, more experimental work might improve the design's form factor by making it smaller and more compact. In addition, by employing the proposed correlation method, the thermal performance of the fan-sink design may be approximated by simple calculations prior to the final design being manufactured.

CONCLUSION

This study proposes a rotating fan-sink. Numerical and experimental fan-sink results are consistent. The thermal resistance of the fan-sink is significantly less than those of the literature (Kim and Kim 2013, Kim et al. 2008, Staats and Brisson 2015,

Koplow 2010, Choi and Jeong 2016).

The effects of several parameters on the performance of the fan-sink are investigated as follows:
(1) The higher number of blades n, the smaller the thermal resistance R_{heat}.
(2) The thermal resistance R_{heat} decreases with increasing power consumption P_{fan} and rotating speed N. Nevertheless, the power consumption or rotating speed exceeds a certain threshold, and the thermal resistance approaches steadily.
(3) The maximum thermal performance of the fan-sink with hub ratio α=2.0 can reach 0.34°C/W at 1200 rpm while it consumes 0.97W of power.
(4) If the hub ratio α of the fan-sink is 1.25, the rotating speed N=900 rpm, and the power consumption P_{fan}=0.38W, its thermal resistance is 0.41°C/W. The corresponding thermal admittance-power consumption ratio is 6.42 and significantly greater than those given by the literature studies.

ACKNOWLEDGMENT

REFERENCES

Abdel-Rehim, Z. S. 2009. "Optimization and Thermal Performance Assessment of Pin-Fin Heat Sinks." *Energy Sources, Part A: Recovery, Utilization and Environmental Effects* 31 (1): 51–65. https://doi.org/10.1080/15567030701468118.

Abed Mohammed Al-Jewaree, H. and Suker, D. K. 2021. "Practical Investigation to Improve the Heat Transfer Performance in Elliptical Fins for Different Axis Ratios by Forced Convection." *American Journal of Mechanical Engineering* 9 (1): 18–23. https://doi.org/10.12691/ajme-9-1-3.

Argyropoulos, C. D., and Markatos, N. C. 2015. "Recent Advances on the Numerical Modelling of Turbulent Flows." *Applied Mathematical Modelling* 39 (2): 693–732. https://doi.org/10.1016/j.apm.2014.07.001.

Choi, J. and Jeong, M. 2016. "Compact, Lightweight, and Highly Efficient Circular Heat Sink Design for High-End PCs." *Applied Thermal Engineering* 92: 162–71. https://doi.org/10.1016/j.applthermaleng.2015.09.096.

Dhaiban, H. and Hussein, M. 2020. "The Optimal Design of Heat Sinks: A Review." *Journal of Applied and Computational Mechanics* 6 (4): 1030–43. https://doi.org/10.22055/jacm.2019.14852.

Huang, C. H., and Gau, C. W. 2012. "An Optimal Design for Axial-Flow Fan Blade: Theoretical and Experimental Studies." *Journal of Mechanical Science and Technology* 26 (2): 427–36. https://doi.org/10.1007/s12206-011-1030-7.

Kim, J. and Kim, S. 2013. "Heat Transfer Characteristics of a Centrifugal Heat Sink." *International Journal of Heat and Mass Transfer* 56 (1–2): 188–96. https://doi.org/10.1016/j.ijheatmasstransfer.2012.09.039.

Kim, T. , Kim, D. and Kim, S. 2008. "Scroll Heat Sink: A Novel Heat Sink with the Moving Fins Inserted between the Cooling Fins." *International Journal of Heat and Mass Transfer* 51 (13–14): 3267–74. https://doi.org/10.1016/j.ijheatmasstransfer.2008.03.014.

Koplow, J. P. 2010. "A Fundamentally New Approach to Air-Cooled Heat Exchangers." California. https://doi.org/https://www.osti.gov/servlets/purl/984140.

Kundu, P. K., Cohen, I. M. and Dowling, D.R. eds. 2012. "Chapter 4 - Conservation Laws." In *Fluid Mechanics (Fifth Edition)*, Fifth Edition, 95–169. Boston: Academic Press. https://doi.org/https://doi.org/10.1016/B978-0-12-382100-3.10004-6.

Lin, S. M., Liu, H. F., Wang, W.R., Lee, S.Y., Cheng, C.Y., and Li, C.Y. 2015. "Optimum Design and Heat Transfer Correlation Equation of a Mini Radiator with Jet Impingement Cooling." *Applied Thermal Engineering* 89: 727–37. https://doi.org/10.1016/j.applthermaleng.2015.06.065.

Menter, F. R. 1994. "Two-Equation Eddy-Viscosity Turbulence Models for Engineering Applications." *AIAA Journal* 32 (8): 1598–1605. https://doi.org/10.2514/3.12149.

Ong, K.S. S., Tan, C.F. F., Lai, K.C. C., and Tan, K.H. H. 2017. "Heat Spreading and Heat Transfer Coefficient with Fin Heat Sink." *Applied Thermal Engineering* 112 (September): 1638–47. https://doi.org/10.1016/j.applthermaleng.2016.09.161.

Staats, W. L., and Brisson, J. G. 2015. "Active Heat Transfer Enhancement in Air Cooled Heat Sinks Using Integrated Centrifugal Fans." *International Journal of Heat and Mass Transfer* 82: 189–205. https://doi.org/10.1016/j.ijheatmasstransfer.2014.10.075.

Taylor, J. R., and Thompson, W. 1998. "An Introduction to Error Analysis: The Study of Uncertainties in Physical Measurements." *Physics Today* 51 (1): 57–58. https://doi.org/10.1063/1.882103.

Yang, Y. T., Lin, S. C., Wang, Y. H., and Hsu, J. C. 2013. "Numerical Simulation and Optimization of Impingement Cooling for Rotating and Stationary Pin-Fin Heat Sinks." *International Journal of Heat and Fluid Flow* 44: 383–93. https://doi.org/10.1016/j.ijheatfluidflow.2013.07.008.

Yoon, Y., Kim, D. R., and Lee, K. S. 2020. "Cooling Performance and Space Efficiency Improvement Based on Heat Sink Arrangement for Power Conversion Electronics." *Applied Thermal Engineering* 164 (April 2019): 114458. https://doi.org/10.1016/j.applthermaleng.2019.114458.

Yunus, C. and Ghajar, A. 2014. *Heat and Mass Transfer: Fundamentals and Applications 5th Edition*. 5th ed. McGraw Hill.

Zhang, S., Lu L., Dong C., and Cha, S.H. 2019. "Performance Evaluation of a Double-Pipe Heat Exchanger Fitted with Self-Rotating Twisted Tapes." *Applied Thermal Engineering* 158 (May): 113770. https://doi.org/10.1016/j.applthermaleng.2019.113770.

創新型旋轉式熱槽散熱器的熱性能

林水木 周新光 廖慶聰
崑山科技大學機械工程學系 綠能科技研究中心*

Agustinus Purna Irawan
塔魯瑪迦大學機械工程學系

摘 要

傳統上冷卻裝置由兩個元件組成：（1）熱槽和（2）軸流風扇。本研究提出了一種新型的旋轉風扇熱槽散熱器設計，由導熱材料製成的旋轉風扇具有兩個功能：熱能的傳導和推動冷空氣中的流動。旋轉風扇熱槽散熱器的電腦模擬數值和實驗結果非常一致。提出了比對本裝置性能的兩個設計指標：（1）盡可能降低熱阻值和（2）盡可能高的速度驅動旋轉風扇下熱導納與所需功耗的比率。通過增加導熱風扇和冷卻空氣的相對速度，可以提高冷卻性能。研究了葉片數量、輪轂直徑和功耗對傳熱性能的影響。本研究發現，在某些參數下，旋轉風扇熱槽散熱器的熱阻遠低於現有文獻。此外，熱導納–功耗比明顯大於其他冷卻裝置。最後，建立了一些Nusselt 數的相關公式，與實驗數據相比誤差小於6%。